ELSEVIER

Materials Science and Engineering A353 (2003) 99–104

MATERIALS SCIENCE & ENGINEERING A

www.elsevier.com/locate/msea

Nanometer-scale solute clustering in aluminum–nickel–ytterbium metallic glasses

Dieter Isheim [a,*], David N. Seidman [a], John H. Perepezko [b], Gregory B. Olson [a]

[a] *Department of Materials Science and Engineering, Northwestern University, 2220 Campus Drive, Evanston, IL 60208-3108, USA*
[b] *Department of Materials Science and Engineering, University of Wisconsin-Madison, 1509 University Av., Madison, WI 53706, USA*

Abstract

The transformation sequence of melt-spun Al–5.2at.% Ni–6.8at.% Yb is characterized by X-ray diffraction, differential scanning calorimetry (DSC), and atom-probe field-ion microscopy. An isochronal DSC thermogram detects three major exothermic transformation steps, with onset temperatures of 180, 292, and 327 °C, respectively. Atom-probe analyses reveal the evolution of compositional inhomogeneities on an atomic scale. In addition to Ni–clusters present in the as-quenched alloy, Ni–Yb co-clusters form during isochronal heating to 188 °C. Al–rich precipitates are detected after heating to 250 °C, with the Ni and Ni–Yb clusters still present, constituting possible precursors of intermetallic phases formed during advanced transformation stages.

Keywords: Amorphous and partially crystallized material; Aluminum–nickel–ytterbium alloy; Clustering

PACS numbers: 61.16.Fk; 61.10.−i; 61.43.Dq; 61.46.+w; 64.60.My; 64.70.Kb; 81.05.Kf; 81.05.Ys; 81.10.Jt; 81.30.Mh; 81.70.Pg

1. Introduction

Al–3D-TM–RE based metallic glasses, where 3D-TM stands for a 3D-transition metal and RE for a rare-earth element, with Al contents of 85–90at.% have attracted interest due to their excellent mechanical properties. A yield strength of 800 MPa has been reported for materials in the amorphous state and an increase of up to 1500 MPa has been observed when the initially amorphous alloys are heat treated and partially crystallized [1,2].

In order to understand the mechanical properties and their changes upon thermal treatments as well as the thermal stability of the resulting microstructure, the chemical and structural changes induced by heat treatments need to be characterized on an atomic scale. Many Al–3D-TM–RE based metallic glasses exhibit a characteristic two-step transformation behavior when heated, usually with the first transformation step related to the formation of Al–rich nanocrystalline grains and the second and subsequent steps related to the formation of intermetallic compounds [1–6]. Additionally, segregation and clustering effects have been reported for partially crystallized Al–Ni–Cu–Ce alloys [7], indicating a complex transformation scheme. Many details of the underlying processes remain unclear and the present study focuses on the microstructural and compositional changes associated with the first transformation step. The transformation behavior of an Al–5.8at.% Ni–6.2at.% Yb alloy is characterized by means of differential scanning calorimetry (DSC), X-ray diffraction (XRD), and atom-probe field-ion microscopy (APFIM). The latter is particularly suitable for the study of small-scale concentration fluctuations, as a spatial resolution of a single atomic layer or 0.2 nm in the depth of the specimen and of 1–2 nm laterally can be achieved. We report the formation of different types of solute clusters that form in the first transformation step as a result of heating.

2. Experimental methods

An alloy ingot with a nominal composition Al–5.2at.% Ni–6.8at.% Yb was prepared by nonconsum-

* Corresponding author. Tel.: +1-847-491-3575; fax: +1-847-467-2669.
E-mail address: isheim@northwestern.edu (D. Isheim).

0921-5093/02/$ - see front matter
doi:10.1016/S0921-5093(02)00674-3

able arc melting in a gettered argon atmosphere and was remelted at least five times to ensure complete alloying. The alloy was subsequently remelted and rapidly quenched in a single roller melt-spinner with a surface speed of the rotating wheel of 55 ms^{-1}, producing ribbons about 1–3 mm wide with an average thickness of 30 μm. The ribbons were cut into snippets about 1×5 mm^2 in area and encapsulated in Al-cartridges for heat treatment in a Perkin-Elmer DSC7. Three different sets of specimens were heated isochronally to 188, 250 or 400 °C, respectively, with a heating rate of 10 °C min^{-1}. XRD was employed for an overall structural characterization.

The local composition was analyzed on a subnanometer scale by APFIM. Needle-shaped specimens for APFIM were prepared in the following way: The heat treated snippets were ground mechanically from the edges to an approximately square cross-section of 30×30 μm^2. During this procedure, the specimens that were heated to 400 or 250 °C were found to be considerably more brittle than the as-quenched material or the one heated to 188 °C. FIM tips were prepared from these blanks by electropolishing in a solution of 2 vol.% perchloric acid in butoxyethanol at 11 V DC.

APFIM was carried out employing a Vacuum Generator FIM100 atom probe. Atom-probe analyses were performed with a pulse-fraction of 20%, a 5 or 50 Hz pulse repetition rate, and a specimen temperature of 25 K in a vacuum of 3×10^{-8} Pa gauge pressure. Pulsed field-evaporation of a specimen under these conditions produces singly and doubly charged Al and Ni ions, whereas ytterbium is observed only in the doubly charged state. The residual partial pressure of hydrogen in the analysis chamber lead to the formation of aluminum hydride complex ions. Fig. 1 displays a mass spectrum obtained for a material that had been heated to 188 °C. Because AlH_2^+ has the same mass-to-charge-state ratio as $^{58}Ni^{++}$, 29 amu, Al hydride formation presents a problem for compositional analyses. In order to minimize hydride formation, the analyses were performed at the instrumental minimum residual gas pressure of $3–5 \times 10^{-8}$ Pa. For determining compositions, the Ni^+ and Al^{++} peaks, which are unambiguous, in the mass spectrum were treated separately from the ambiguous peaks. By using the tabulated natural isotopic abundances of the five stable Ni isotopes and comparing them with the recorded spectrum, Fig. 1, the relative contribution of AlH_x^+ and Ni^{++} could be assessed. Only if the Al hydride contribution was smaller than 15% were these peaks assigned to Ni, otherwise they were treated separately.

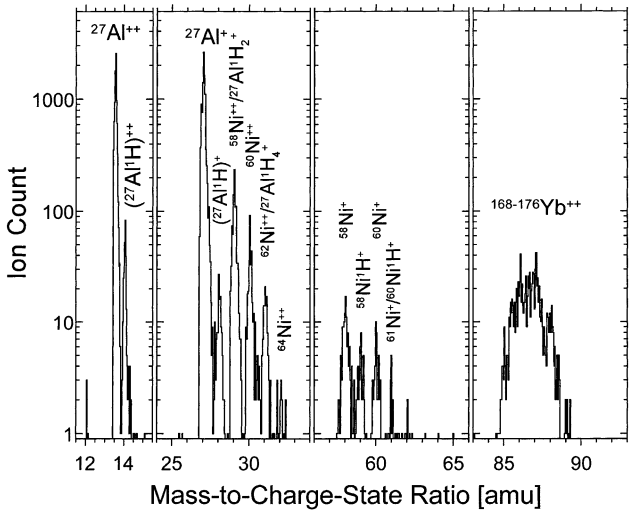

Fig. 1. Atom-probe time-of-flight mass spectrum of an Al–5.2at.% Ni–6.8at.% Yb alloy heated isochronally to 188 °C at a rate of 10 °C min^{-1}.

3. Results

3.1. Differential scanning calorimetry

Isochronal heating to 400 °C at a rate of 10 K min^{-1} yields the thermogram shown in Fig. 2. Two heating runs were performed under identical conditions, the second one being carried out with the completely transformed sample. In order to obtain the absolute heating power, the second run was subtracted from the first one. The result is shown in Fig. 2. This thermogram features three major exothermic peaks, or heat releases, corresponding to transformation steps I, II and III, as indicated in Fig. 2. Heat release I has an onset temperature of 180 °C, release II begins at 292 °C, and release III has an initiation temperature of 327 °C. In order to characterize the microstructural changes occurring during step I, one set of specimens was heated

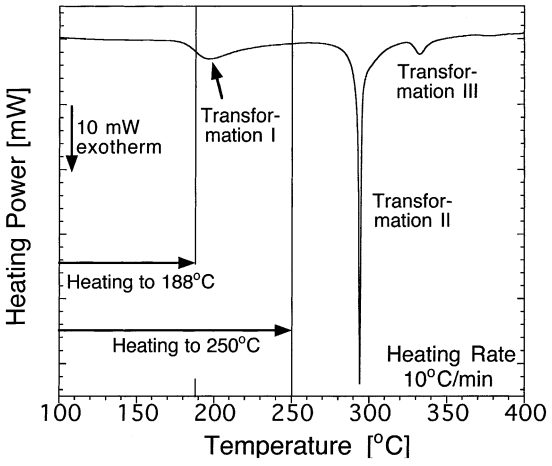

Fig. 2. Differential scanning calorimetry thermogram of melt-spun Al–5.2at.% Ni–6.8at.% Yb. The heating rate is 10 °C min^{-1}. The transformation stages investigated in this study, at the beginning of transformation I and with transformation I completed, are indicated.

to 188 °C at a rate of 10 °C min^{-1}, corresponding to the beginning of the transformation with about 15% of this transformation's enthalpy released, and a second set of specimens was heated to 250 °C, representing a completed transformation step I.

3.2. X-ray diffraction

Fig. 3 displays X-ray diffractograms for the as-quenched state and material heated to 188 or 250 °C at a rate of 10 K min^{-1}. The as-quenched state is characterized by a broad maximum centered around $2\theta = 38°$, revealing that the dominant part of the material is amorphous. At a diffraction angle of $2\theta = 38.4°$, a small sharp peak is discernible, implying that crystalline grains are present with a small volume fraction. Heating to 188 °C increases the relative height of this small sharp peak slightly, indicating a small increase in the volume fraction of the crystalline phase. Heating to 250 °C produces strong diffraction peaks with a distinct pattern of an fcc structure, while the broad maximum demonstrates that a significant volume fraction still has an amorphous structure. A comparison of the peak positions with the Bragg angles of pure Al, see Fig. 3, reveals a deviation toward smaller Bragg angles. The peak positions correspond to a lattice parameter of 0.4077 ±0.005 nm, which means a lattice expansion of about 0.7% as compared to pure Al with a lattice parameter of 0.40496 nm [8], most likely due to solute atoms and structural defects.

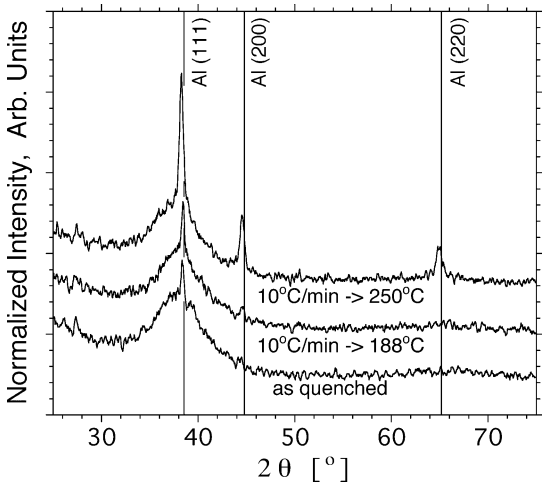

Fig. 3. X-ray diffractograms of melt-spun Al–5.2at.% Ni–6.8at.% Yb in the as-quenched state and heated to 188 or 250 °C, respectively, at a rate of 10 °C min^{-1}, employing Cu-Kα-radiation. The intensities are normalized by the integral intensity of the respective first, dominant peak. The positions of the Bragg peaks of pure Al are marked by vertical lines.

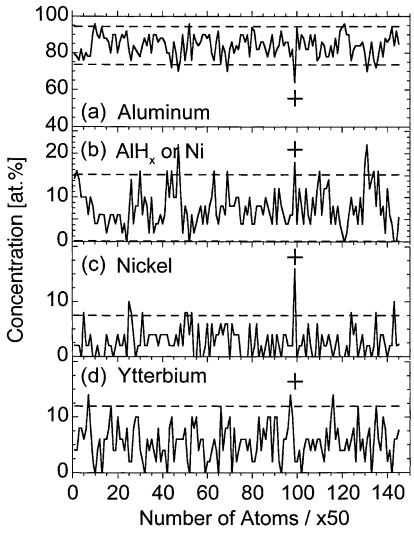

Fig. 4. Ni–rich cluster (+) in an atom-probe concentration profile of melt-spun Al–5.2at.% Ni–6.8at.% Yb in the as-quenched state. The horizontal dashed lines in each concentration profile are the two-sigma limits of a random concentration distribution with the same average composition and block size, encompassing an average 96% of the measured values. Concentration peaks distinctively exceeding the dashed lines are significant.

3.3. Atom-probe analyses

Fig. 4 is an atom-probe concentration profile into the depth of as-quenched material with a random starting position. The concentration values are calculated from blocks of 50 atoms. The projected diameter of the aperture limiting the analyzed area is about 2 nm in the beginning of the analysis, and about 3 nm at the end. The composition profile treats atoms with mass-to-charge-state ratios in the critical AlH_x/Ni^{++} range separately because the aluminum hydride complex ions essentially mask the doubly-charged nickel ions. Ni^+ as well as Al^+ and all ytterbium ions, however, can be identified unambiguously, allowing for the detection of inhomogeneities in spite of the hydride problem. The horizontal dashed lines in each concentration profile are the 2σ limits of a random concentration distribution with the same average composition and block size, encompassing about 96% of the measured values, i.e. concentration peaks distinctively exceeding the dashed lines are significant. The profiles reveal a Ni–rich cluster, labeled with a cross in Fig. 4. The compositions of Ni–rich clusters and the matrix are given in Table 1. As the diameter of the projected aperture is probably larger than the diameter of a cluster with 30–50 detected atoms, reflecting a detection efficiency of about 50%, this number of atoms corresponds to a cluster size of about 1 nm diameter; the measured Ni concentration is a lower limit for the true value. Clusters of this size can be resolved by the atom probe at all due to the fact that atoms are field evaporated in clusters rather than perfectly uniform across the analyzed area.

Table 1
Compositions of a Ni–rich cluster and the amorphous matrix in as-quenched Al–5.2at.% Ni–6.8at.% Yb

		Al	AlH_x or Ni	Ni	Yb
Matrix	Number of atoms	6110	549	197	403
	composition (at.%)	84.0±0.4	7.6±0.3	2.8±0.2	5.5±0.3
Ni–rich cluster	Number of atoms	16	7	8	1
	composition (at.%)	50±9	22±7	25±8	3±3

The error in the concentration, c, is the statistical error $\sigma_c = \sqrt{c(1-c)/N}$, with N being the total number of atoms detected.

Material heated to 188 °C, corresponding to the early stages of transformation I, shows a much more inhomogeneous distribution of the constituents. The concentration profile in Fig. 5 contains a large number of clusters enriched in nickel *and* ytterbium, which are labeled with a solid diamond, in addition to a few Ni–rich clusters, marked with a cross. One potential Yb–rich cluster, labeled O in Fig. 4, is statistically not significant. The apparent compositions of the different types of clusters and the matrix are given in Table 2. The aluminum hydrides contribute only approximately 10–20% of the total Ni count; therefore they are not listed separately, but combined with Ni events. Overall, the Ni concentration is, overestimated by about 10–20%.

Fig. 6 is a multicomponent integral concentration profile of two Ni–Yb co-clusters from the concentration profile shown in Fig. 5. The integral number of detected Al, Ni, Yb, or AlH_x or Ni atoms is plotted versus the total number of all detected atoms. Consequently, the local slope yields directly the local concentration of the respective species. This diagram distinguishes between Ni atoms unambiguoulsy identified in the mass spectrum and the atoms affected by the $A1H_x$/Ni mass overlap. This diagram proves that the Ni–Yb co-clusters can be identified clearly, in spite of the presence of aluminum hydrides.

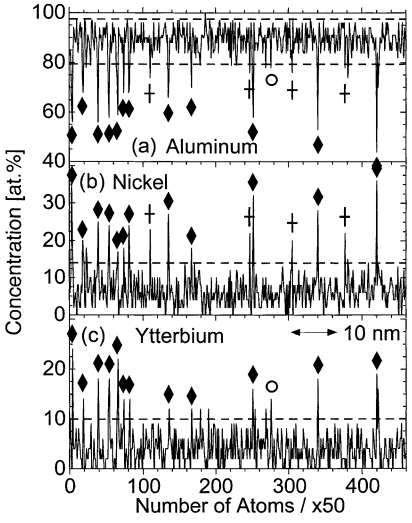

Fig. 5. Yb–Ni co-clusters (◆), Ni–rich clusters (+), and one potential Yb cluster (○) in an atom-probe concentration profile of melt-spun Al–5.2at.% Ni–6.8at.% Yb heated to 188 °C at a rate of 10 °C min^{-1}. The horizontal dashed lines in each concentration profile are the two-sigma limits of a random concentration distribution with the same average composition and block size, encompassing an average 96% of the measured values, i.e. concentration peaks distinctively exceeding the dashed lines are significant. The scale bar is approximate.

Fig. 7 displays a random area concentration profile obtained on material heated up to 250 °C with a completed transformation I. The profile contains two Al–rich precipitates, labeled by an open square, with an estimated size of 2–4 nm. Additionally, small Ni–clusters and Ni–Yb co-clusters are present, indicated by crosses and diamonds, respectively, similar to the clusters detected in material of the early stage of transformation I. At the rear interface of the first A1–rich precipitate there is a significant enrichment in ytterbium, labeled with an open circle. There is no apparent spatial correlation of the two Al precipitates with the Ni–Yb co-clusters. The average compositions of Al-rich precipitates, Ni, and Ni–Yb co-clusters are listed in Table 3.

4. Discussion

The three investigated transformation stages of melt-spun Al–5.2at.% Ni–6.8at.% Yb, as-quenched and heated with a rate of 10 K min^{-1} to 188 or 250 °C, respectively, reveal a remarkable transformation sequence in this alloy. A Ni–rich cluster, smaller than about 1 nm in diameter is found in the as-quenched state. XRD demonstrates the presence of Al–rich crystallites already in the as-quenched state; the small and comparatively sharp (1 1 1) Bragg reflection, however, indicates a size of at least several tens of nanometers with a small volume fraction, which explains why these Al–rich crystallites are not detected with the atom-probe. Heating to 188 °C produces a large number of clusters enriched in Ni and Yb, with an average composition $A1_{59}Ni_{25}Yb_{17}$ (at.%). The atom-probe also detects Ni–rich clusters with the approximate

Table 2
Compositions of clusters and matrix in Al–5.2at.% Ni–6.8at.% Yb heated isochronally to 188 °C at a rate of 10 °C min^{-1}

		Al	Ni	Yb
Matrix	Number of atoms	19937	1332	403
	average composition (at.%)	90.1±0.2	6.0±0.2	3.9±0.1
6 Ni–rich clusters	Number of atoms	126	74	8
	average composition (at.%)	60.6±3.4	35.6±3.3	3.9±1.3
13 Ni and Yb–rich co-clusters	Number of atoms	452	190	128
	average composition (at.%)	58.7±1.8	24.7±1.6	16.6±1.3

The error in the concentration c is the statistical error $\sigma_c = \sqrt{c(1-c)/N}$, with N being the total number of atoms detected.

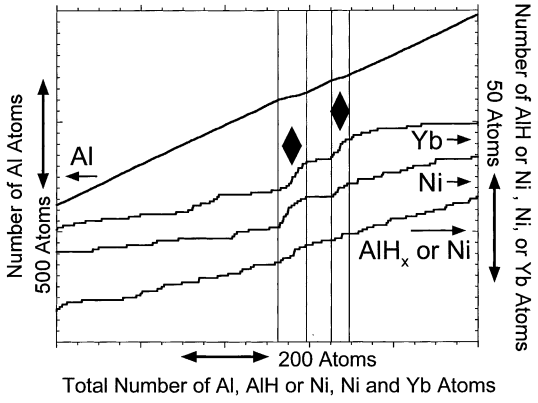

Fig. 6. Yb–Ni co-clusters (◆) in a multicomponent integral concentration profile for Al, Yb, Ni, and AlH$_x$ or Ni of melt-spun Al–5.2at.% Ni–6.8at.% Yb heated to 188 °C at a rate of 10 °C min^{-1}. The clusters can safely be recognized, in spite of a convolution of the Ni$^+$-peaks in the mass spectrum by the formation of AlH$_x^+$ complex ions during pulsed field evaporation.

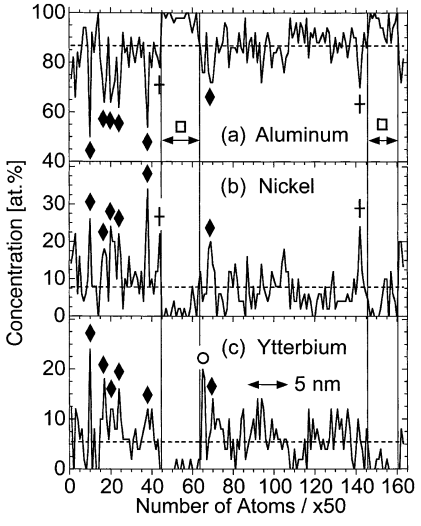

Fig. 7. Yb–Ni co-clusters (◆), Ni–rich clusters (+), and Yb–cluster (○) in a multicomponent atom-probe concentration profile of melt-spun Al–5.2at.% Ni–6.8at.% Yb heated to 250 °C at a rate of 10 °C min^{-1}. The horizontal dashed lines are the concentrations averaged over the entire profile.

composition $Al_{61}Ni_{36}Yb_4$ (at.%), which is, within the error limits, similar to the composition of the Ni–rich cluster found in the as-quenched state. The X-ray diffractogram of this stage is very similar to the one of the as-quenched state, with the slightly increased relative height of the (1 1 1) reflection indicating a slightly increased volume fraction of the crystalline fraction.

Heating to 250 °C generates small Al–rich precipitates as detected with the atom-probe, concomitant with a significant increase in intensity of the (1 1 1) reflection in the diffractogram. Ni–rich clusters and Ni–Yb co-clusters are present, with an average composition of $Al_{69}Ni_{25}Yb_4$ or $Al_{61}Ni_{25}Yb_{14}$ (at.%), respectively. These compositions are very similar to the ones measured for the clusters in material heated to 188 °C. It is thus concluded that the clusters formed during heating into the beginning of transformation step I remain unchanged by the further progress of this transformation. The first Al–rich precipitate in the concentration profile shown in Fig. 7 is flanked by a Ni–cluster at the front interface and by a Yb–cluster at the back side. With the caveat that only two Al–rich precipitates have been found, this indicates that the Ni–Yb co-clusters do not provide the nucleation sites for the Al–rich precipitates. The stability of the Ni–Yb co-clusters through transformation step I, however, suggests that they persist to higher temperatures and may play an important role for the formation of binary or ternary intermetallic phases during the transformation steps at higher temperatures.

5. Conclusion

The microstructural changes and partitioning processes of melt-spun Al–5.2at.% Ni–6.8at.% Yb have been followed in detail through the first of three transformation steps detected by significant heat releases in a DSC thermogram recorded by isochronal heating. Additional to Ni–clusters present in the as-quenched alloy, Ni–Yb co-clusters form during iso-

Table 3
Compositions of Al–rich precipitate, clusters and matrix in Al–5.2at.% Ni–6.8at.% Yb heated isochronally to 250 °C at a rate of 10 °C min^{-1}

		Al	Ni	Yb
Matrix	Number of atoms	4680	396	332
	average composition (at.%)	86.5±0.5	7.3±0.4	6.1±0.3
2 Ni–rich clusters	Number of atoms	76	31	4
	average composition (at.%)	68.5±4.4	27.9±4.3	3.6±1.8
6 Ni and Yb–rich co-clusters	Number of atoms	287	115	67
	average composition (at.%)	61.2±23	24.5±2.0	14.3±1.6
Yb–rich cluster at Al–rich precipitate	Number of atoms	73	5	19
	average composition (at.%)	75.3±4.4	5.1±2.2	19.6±4.0
Al–rich precipitate	Number of atoms	764	8	3
	average composition (at.%)	98.6±0.4	1.0±0.4	0.4±0.2

The error in the concentration c is the statistical error $\sigma_c = \sqrt{c(1-c)/N}$, with N being the total number of atoms detected.

chronal heating to 188 °C. Al–rich precipitates are detected by atom-probe analysis after heating to 250 °C, with the Ni and Ni–Yb clusters still present, constituting possible precursors of intermetallic phases formed during later transformation stages.

Acknowledgements

The authors wish to thank Dr R. Wu for preparing and precharacterizing the investigated alloy. This research was supported by the Department of Defense through the DARPA initiative under contract number DAAH01-01-C-R009 (D.I., D.N.S., and G.B.O.) and DAAD19-01-1-0486 (J.H.P.).

References

[1] Y.-H. Kim, A. Inoue, T. Masumoto, Mater. Trans. JIM 32 (1991) 599.
[2] A. Inoue, Y.-H. Kim, T. Masumoto, Mater. Trans. JIM 33 (1992) 487.
[3] K. Nakazato, Y Kawamura, A.P. Tsai, A. Inoue, T. Masumoto, Appl. Phys. Lett. 63 (1993) 2644.
[4] Y.-H. Kim, A. Inoue, T. Masumoto, Mater. Trans. JIM 31 (1990) 747.
[5] A. Inoue, Y Horio, Y.-H. Kim, T. Masumoto, Mater. Trans. JIM 33 (1992) 669.
[6] A. Inoue, K. Nakazato, Y. Kawamura, A.P. Tsai, T. Masumoto, Mater. Trans. JIM 35 (1994) 95.
[7] K. Hono, Y. Zhang, A.P. Tsai, A. Inoue, T. Sakurai, Scripta Metall. Mater. 32 (1995) 191.
[8] T.B. Massalski (Ed.), Binary Alloy Phase Diagrams, American Society of Metals, Metals Park, OH, 1986.